GPS Solutions (2024) 28:53
https://doi.org/10.1007/s10291-023-01592-5

ORIGINAL ARTICLE

Linear quadratic Gaussian-based clock steering system for GNSS real-time precise point positioning timing receiver

Wenfei Guo[1] · Mengmeng Zhu[1] · Shengfeng Gu[1] · Hongming Zuo[1] · Jingnan Liu[1]

Received: 6 February 2023 / Accepted: 28 November 2023 / Published online: 29 December 2023
© The Author(s), under exclusive licence to Springer-Verlag GmbH Germany, part of Springer Nature 2023

Abstract

Clock steering is crucial for Global Navigation Satellite System (GNSS) timing receivers to provide high-performance time and frequency. However, the lack of theoretical analysis and design methods makes it difficult to apply an existing controller to the emerging real-time precise point positioning (RT-PPP) timing receiver. In this research, a Linear Quadratic Gaussian (LQG)-based clock steering method for the RT-PPP timing receiver is proposed with a detailed design process. We theoretically derive the transfer function of the system first. Then, the relationship between the system bandwidth and the control parameter is present. As for the parametric design, based on the analysis of the free-running oscillator instability, the RT satellite clock reference variation, and the GNSS observation noise, the parameters of the Kalman estimator are set, and the optimal bandwidth of the system is estimated. Under the constraint of the bandwidth and the damping ratio, the control parameters of the LQG controller are determined finally. Simulated results show that the parametric design method is feasible for different noise conditions. And finally, we evaluate the performance of the proposed clock steering method on a Rubidium clock RT-PPP timing receiver. Experimental results show that the timing receiver realizes the optimal combination of the short-term stability of the Rubidium clock and the long-term stability of the RT-PPP reference expectedly. The precision of the output one pulse per second (1PPS) is 0.21 ns over 24 h. And the frequency stabilities can reach 3.59E-12@1s and 2.43E-14@10000s, which is more stable than a high-quality Cesium clock.

Keywords Timing receiver · LQG · Clock steering · Parameter design

Introduction

In addition to positioning and navigation applications, Global Navigation Satellite Systems (GNSS) are commonly used to provide wide-area, low-cost, and high-precision time and frequency. As generated by the atomic clocks onboard satellites and designed to range between the satellites and the receivers, GNSS signals contain embedded timing information that can distribute accurate time and frequency. However, GNSS receivers, as the terminals, are often equipped with lost cost oscillators, such as temperature-compensated crystal oscillators, oven-controlled crystal oscillators, and chip scale atomic clocks. These oscillators diverge over time due to internal noises. Thus, GNSS receivers need to carefully steer the clock regularly according to the GNSS observation and keep the time and frequency consistent with the RT satellite clock reference.

The design of a clock steering strategy is essentially a feedback control problem for a dynamic system. The first step to realizing a satisfactory feedback system is to understand the process and translate dynamic performance requirements into time and frequency or pole-zero specifications (Franklin et al. 2002). Frequency stability is an important requirement for timing applications, which can be specified and measured with both the Allan Deviations (ADEV) in the time domain and the power spectral density (PSD) in the frequency domain (Riley and Howe 2008). Due to the mature theory, Phase-Lock Loop (PLL) was first used to lock the local time to the GNSS time (Kusters 1996). In a PLL clock steering system, the dynamic performance requirements of frequency stability are translated into specifications in the frequency domain (Hajimiri 2001). Thus, the noises of the PLL system are researched to generate a desirable time scale. Gardner (2005) summarized the phase-lock techniques and pointed out that the bandwidth of a PLL

✉ Shengfeng Gu
gsf@whu.edu.cn

[1] GNSS Research Center, Wuhan University, Louyu Road 129, Wuhan 430079, Hubei, China

should be a trade-off to minimize the total phase jitter. Wu et al. (2016) simulated the bandwidth design of the DPLL system to steer a Hydrogen maser to a Cesium clock. PLL is a simple and practical system for clock steering, which, however, is not flexible enough to meet the requirements of a high-precision timing receiver, for only its bandwidth could be changed.

Similar dynamic performance requirements are also considered in the modern control theory. Linear Quadratic Gaussian (LQG) is a well-known modern controller. Koppang and Leland (1999) successfully used the LQG to steer a remote Hydrogen maser to the UTC(USNO) within several nanoseconds without reducing its stability. However, the designed parameters are not generic in other applications, for they were chosen according to numerical simulations. Koppang (2003) applied the control theory in the formation of a stable atomic timescale that combines the short-term stability of the Hydrogen masers and the long-term stability of the Cesium frequency standards. The control law of the LQG controller was redesigned using the Pole-Placement (PP) technique. And the stability improvement was verified with the simulated results. Matsakis (2019) extended Koppang's analyses and unified the PP and LQG techniques, which can turn the design of the weight matrices of the LQG to the time constant in the PP. While the chosen method of the time constant was not specified. For the first time, Mishagin (2019) proposed a practical design method of the time constant according to the cross point of Allan deviations of the reference clock and the free-running oscillator. In the derivation, however, a linear scale coefficient was introduced for the time constant determination, which makes the method not so clear. In fact, the bandwidth is more important than the time constant with the requirements of the combined stabilities of the reference and the controlled oscillator.

In recent years, with the development and maturity of real-time precise point positioning (RT-PPP), the performance of GNSS positioning (Ramachandran et al. 2019) and timing (Guo et al. 2019) are both significantly improved. With regards to time and frequency transfer, the stability of the RT-PPP satellite clock reference can reach 6–8E-15@1day (Guo et al. 2022), which has great potential for high-precision timing. As for real-time applications, Rønningen and Danielson (2019) demonstrated that real-time GNSS corrections can realize low-cost time/frequency distribution with stability surpassing high-performance industrial Cesium clocks. Guo et al. (2019) realized an RT-PPP timing receiver using an OCXO with the timing precision of sub-nanosecond and the stability of 2E-14@1 day. In such an RT-PPP timing receiver, the divergence of the oscillator is monitored by the RT-PPP observation and corrected by the clock steering system. Then, the time and frequency could be synchronized to the reference. Different from the combination of two atomic clocks in the time and frequency laboratory, the observation of RT-PPP timing receivers has non-neglected fluctuations due to complex environments of GNSS signal propagation. It was found that the fluctuations of the RT-PPP time transfer could cause the clock excessively steered, resulting in a loss of short-term frequency stability. Thus, the clock steering needs to be carefully designed so that the steered oscillator can give reasonable frequency stability both in the short-term and long-term.

To improve the performance of frequency stability of the RT-PPP timing receiver, a clock steering method based on LQG is proposed in this article. The characteristics and parameter design of the clock steering system are emphasized with a practical RT-PPP timing receiver. The entire RT-PPP timing receiver was designed and realized by our group (Guo et al. 2019). And we have studied the effect of the RT-PPP part on timing (Guo et al. 2022). Furthermore, in this paper, we are focusing on the clock steering part. In the next section, we describe the control model of the RT-PPP timing receiver with an LQG controller. Then, we present the LQG controller parameter design method to give optimal frequency stability. And we carry out the clock steering simulations and practical verifications on an RT-PPP timing receiver with a Rubidium clock. Finally, we summarize this article and draw conclusions.

Control model of the RT-PPP timing receiver

Figure 1 shows the structure of an RT-PPP timing receiver. As shown in the figure, the oscillator provides the clock signal to the radio frequency (RF) frontend and baseband processor of the receiver. The radio frequency frontend down converts the frequency of received GNSS signals to the baseband, which is then demodulated by the baseband processor to produce observation and broadcast ephemeris of all visible satellites. The RT-PPP algorithm estimates the clock offset of the receiver using the observation and precise ephemeris. It is worth noting that the RT-PPP precise ephemeris corrections introduce its clock virtual datum. Thus, the evaluated receiver clock offset here is the time

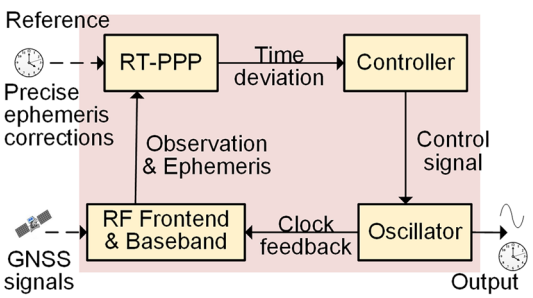

Fig. 1 Structure of the RT-PPP timing receiver

deviation of the receiver clock compared to the RT-PPP satellite clock reference. With the time deviation, the controller produces a frequency control signal, which is used to steer the receiver clock to match the RT-PPP reference clock. Moreover, the steered clock is used as feedback to the receiver as well. As a result, the receiver can provide an accurate time pulse and frequency to the users.

Considering the control requirement of the timing receiver, an LQG controller is introduced for clock steering in this work, which is a universal controller designed in state space, including a Kalman estimator and a linear control law designed by the Linear Quadratic Regulator (LQR) method (Koppang and Leland 1999). Figure 2 shows the RT-PPP timing receiver with an LQG controller. The Kalman estimator filters the time deviation e measured by the RT-PPP and realizes the optimal estimation of the state vector $\hat{\mathbf{x}}$. Then the estimated state vector is multiplied by the control law $-\mathbf{G}$ to calculate the control signal u, with which the oscillator is finally steered. The steered clock is provided to the signal processing process for the RT-PPP measurement as feedback and improves the performance of the RT-PPP timing.

The state equation of the clock steering system can be expressed as follows:

$$\mathbf{x}(n) = \mathbf{A}\mathbf{x}(n-1) + \mathbf{B}u(n-1) + \mathbf{w}(n) \tag{1}$$

$$\mathbf{x}(n) = \begin{bmatrix} \Delta t(n) \\ \Delta f(n) \end{bmatrix}, \mathbf{A} = \begin{bmatrix} 1 & \tau_0 \\ 0 & 1 \end{bmatrix}, \mathbf{B} = \begin{bmatrix} \tau_0 \\ 1 \end{bmatrix} \tag{2}$$

Here the state vector variables $\Delta t(n)$ and $\Delta f(n)$ represent the time and fractional frequency deviation of the receiver clock compared to the RT-PPP reference clock at the epoch n, respectively. $\mathbf{A}$ is the state transition matrix, $\mathbf{B}$ is the input matrix, τ_0 is the sampling interval of the control system, and $u(n-1)$ is the fractional frequency step applied to the oscillator at the epoch $n-1$. $\mathbf{w}(n)$ represents the noise vector with a covariance matrix $\mathbf{Q}$. And the measurement equation of the system is

$$e(n) = \mathbf{C}\mathbf{x}(n) + v(n) \tag{3}$$

where $e(n)$ is the time deviation measured by the RT-PPP at the time n, $\mathbf{C} = \begin{bmatrix} 1 & 0 \end{bmatrix}$ is the observation matrix, and $v(n)$ is the measurement noise variable with a variance R.

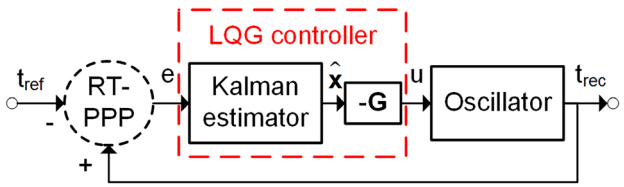

Fig. 2 Control structure of the RT-PPP timing receiver

When the RT-PPP timing receiver is regarded as a control system, the RT-PPP algorithm plays a role as the sensor. The RT-PPP introduces the reference clock and includes the observation noise, which are the important characteristics of the control system. Once the RT-PPP solution strategies related to these characteristics are determined, such as the adoption of satellite systems and precise ephemeris products (Guo et al. 2022), the LQG controller should be designed according to the RT-PPP. Besides the $\mathbf{Q}$ and R of the estimator being calculated to match these characteristics, the control law should also be designed carefully to utilize the high performance of the RT-PPP. This article aims to design the LQG controller based on these RT-PPP characteristics evaluated.

The LQG controller includes a Kalman estimator and a linear LQR control law. According to the standard Kalman Filter iterative formula, the optimal estimation of the state vector $\hat{\mathbf{x}}(n)$ can be derived (Koppang and Leland 1999):

$$\hat{\mathbf{x}}(n) = (\mathbf{I} - \mathbf{K}(n)\mathbf{C})(\mathbf{A} - \mathbf{B}\mathbf{G})\hat{\mathbf{x}}(n-1) + \mathbf{K}(n)e(n) \tag{4}$$

Here $e(n)$ is the measured RT-PPP time deviation, and $\mathbf{K}(n)$ is the Kalman gain. The steady-state Kalman gain is determined by the state covariance matrix $\mathbf{Q}$ and the measurement variance R. $(\mathbf{I} - \mathbf{K}(n)\mathbf{C})(\mathbf{A} - \mathbf{B}\mathbf{G})$, $\mathbf{K}(n)$, represent state transition matrix and input matrix of the LQG controller, respectively.

With the state vector $\hat{\mathbf{x}}(n)$ estimated by the Kalman estimator, the linear LQR control law $-\mathbf{G}$ is used to output fractional frequency step $u(n)$ as follow:

$$u(n) = -\mathbf{G}\hat{\mathbf{x}}(n) \tag{5}$$

Here $-\mathbf{G} = -\begin{bmatrix} g_1 & g_2 \end{bmatrix}$ represents output matrix of the LQG controller and is designed by the LQR method. The LQR-designed control law minimizes the quadratic cost function of the state vector $\mathbf{x}(n)$ and the control variable $u(n)$,

$$J = \sum_{n=0}^{\infty} \left(\mathbf{x}(n)^T \mathbf{W}_x \mathbf{x}(n) + u(n)^T \mathbf{W}_u u(n) \right) \tag{6}$$

$$\mathbf{W}_x = \begin{bmatrix} p & 0 \\ 0 & q \end{bmatrix}, \mathbf{W}_u = r \tag{7}$$

where $\mathbf{W}_x$ and $\mathbf{W}_u$ are state cost matrix and control cost matrix, respectively. The cost matrices have three cost parameters to be designed in, namely p, q and r. Only two of the three cost parameters are independent, i.e., an overall scaling of the three parameters does not affect the minima. And p has dimension of τ_0^{-2}, while r and q are both dimensionless (Matsakis 2019). When $\mathbf{W}_x$ and $\mathbf{W}_u$ are chosen, the control law can be determined,

$$\mathbf{G} = \left(\mathbf{W}_u + \mathbf{B}^T\mathbf{L}\mathbf{B}\right)^{-1}\mathbf{B}^T\mathbf{L}\mathbf{A} \tag{8}$$

$$\mathbf{L} = \mathbf{W}_x + \mathbf{A}^T\mathbf{L}\mathbf{A} - \mathbf{A}^T\mathbf{L}\mathbf{B}\left(\mathbf{W}_u + \mathbf{B}^T\mathbf{L}\mathbf{B}\right)^{-1}\mathbf{B}^T\mathbf{L}\mathbf{A} \tag{9}$$

here $\mathbf{L}$ is a solution to the steady-state Riccati equation. Thus, $\mathbf{W}_x$ and $\mathbf{W}_u$ are the LQR control law parameters to be designed. The goal of parameter design is to reach the optimal frequency stability combination of the free-running oscillator in the short-term and the RT-PPP in the long-term. To design the parameters, we will analyze the system in the frequency domain in the next section and derive the relationship between the fluctuations and the LQG parameters.

Parameter design of the clock steering system

As discussed above, the LQG controller consists of the estimator and the control law, which are supposed to be considered together with regard to the parameter design. According to the separation principle, however, it is reasonable and practical to consider the two parts, respectively. In this section, we will derive the transfer function of the clock steering system and analyze the system in the frequency domain. And then the parameters of the Kalman estimator and LQR control law are discussed in the time and frequency domain respectively.

System analysis in the frequency domain

GNSS RT-PPP timing receiver uses clock steering to integrate the frequency stabilities of its oscillator and the reference, resulting in a stable frequency both in the short- and long-term. The steered clock is expected to have the short-term stability of the free-running oscillator and the long-term stability of the RT-PPP. The instabilities of a frequency source can be specified and measured both in the time domain with the ADEV and in the frequency domain with PSD. That means, the specifications are equivalent in the two domains. Thus, the clock steering goal can also be described as the receiver clock having the high-frequency PSD of the free-running oscillator and the low-frequency PSD of the RT-PPP.

Typically, the fluctuations of the free-running oscillator are smaller than the RT-PPP only over a short time, i.e., the oscillator has smaller PSD than the RT-PPP only in the high-frequency band. In this situation, there should be a point of intersection frequency f_c of the PSD of the RT-PPP's fluctuations and the free-running oscillator's fluctuations (see Fig. 3). Thus, from the filter point of view in frequency domain, the clock steering system is supposed to be a low-pass filter (LPF), whose input is the measurement of RT-PPP. And the

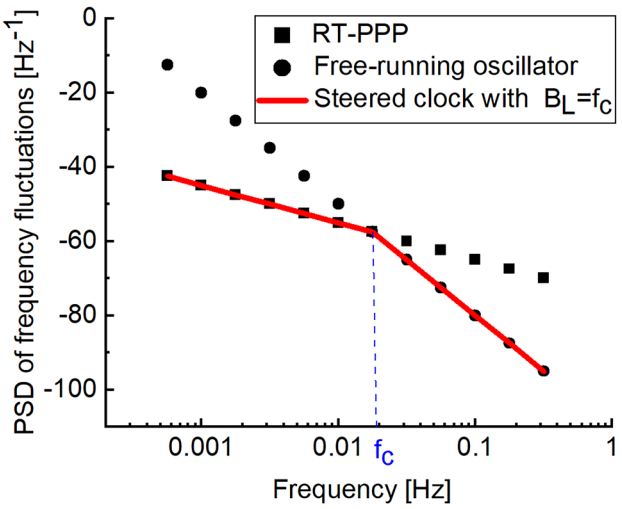

Fig. 3 Ideal power spectral density of steered clock

bandwidth of the filter should be the point of intersection frequency f_c. According to the propagation theory of the fluctuations in the LPF system (Kroupa 1982), the fluctuations of the receiver output frequency comes from the fluctuations of RT-PPP within the low-pass bandwidth B_L, and the fluctuations of the free-running oscillator outside the low-pass bandwidth. As shown in Fig. 3, when the bandwidth B_L is set to the intersection frequency f_c, the receiver clock will have the minimum fluctuations over the whole frequency band.

The transfer function of a state space system can be derived with the state transition matrix, the input matrix, and the output matrix. From Fig. 2, we can see the clock steering system consists of a discriminator named RT-PPP, an LQG controller, and an oscillator. With the time deviation e evaluated by RT-PPP, the LQG controller calculates control signal u to steer the oscillator. The transfer function of the LQG controller can be obtained from Eqs. (4) and (5),

$$\begin{aligned} \boldsymbol{H}_{\mathrm{LQG}}(z) &= \frac{u(z)}{e(z)} \\ &= -\mathbf{G}(z\mathbf{I} - (\mathbf{I} - \mathbf{K}\mathbf{C})(\mathbf{A} - \mathbf{B}\mathbf{G}))^{-1}\mathbf{K}z \\ &= \frac{-z^2(g_1k_1 + g_2k_2) + z(g_1k_1 - g_1k_2\tau_0 + g_2k_2)}{z^2 - z((1-k_2\tau_0)(1-g_2) + (1-k_1)(1-g_1\tau_0)) + (1-k_1)(1-g_2)} \end{aligned} \tag{10}$$

here $\mathbf{K} = \begin{bmatrix} k_1 & k_2 \end{bmatrix}^T$ is the constant vector to which the Kalman gain K(n) converges at steady state.

Using u as the input, the oscillator is steered to produce the expected time and frequency, which is used as the output of the timing receiver and as a feedback to the baseband. The transfer function of the oscillator can be derived from (1) and (3),

$$\boldsymbol{H}_{\mathrm{OSC}}(z) = \frac{t_{\mathrm{rec}}(z)}{u(z)} = \mathbf{C}(z\mathbf{I} - \mathbf{A})^{-1}\mathbf{B} = \frac{z\tau_0}{(z-1)^2} \tag{11}$$

here, **A**, **B**, **C** represent state transition matrix, input matrix, and output matrix of the oscillator, respectively.

When the steered oscillator is used to provide clock to the baseband, the whole clock steering system forms a closed loop. And the closed-loop transfer function of the system can be presented as,

$$\begin{aligned} \boldsymbol{H}(z) &= \frac{t_{\mathrm{rec}}(z)}{t_{\mathrm{ref}}(z)} \\ &= \frac{-H_{LQG}(z)H_{\mathrm{OSC}}(z)}{1-H_{LQG}(z)H_{\mathrm{OSC}}(z)} \\ &= \frac{z^2\tau_0\left(z\left(g_1k_1+g_2k_2\right)-g_1k_1+g_1k_2\tau_0-g_2k_2\right)}{\left(z^2+\left(k_1+k_2\tau_0-2\right)z+1-k_1\right)*\left(z^2+\left(g_2+g_1\tau_0-2\right)z+1-g_2\right)} \end{aligned} \tag{12}$$

As can be seen from the equation above, the transfer function of the system is mainly decided by the Kalman gain and the control law. And moreover, the poles of the estimator and the control law are separated. Thus, the estimator and control law design can be realized, respectively, according to the separation principle in the control theory (Franklin et al. 1998).

Parameters of the clock steering system

With regards to Kalman estimator, the state-driven noise covariance matrix is often designed in the time domain according to the clock noise. The fractional frequency fluctuations of a clock are described by its single sideband power spectrum density, which can be modeled by a combination of power-law noises (Riley and Howe 2008),

$$S_y(f) = \sum_{\alpha=-2}^{2} h_\alpha f^\alpha \tag{13}$$

where f is the sideband Fourier frequency in Hertz, $S_y(f)$ is the PSD of the fractional frequency fluctuations, α is the power-law exponent, and h_α is the power-law noise level figure. A power-law noise with α satisfies $S_y(f) \propto f^\alpha$. The power-law noise with different α dominates over different frequency band, specifically, the power-law noise with a smaller α dominates over the lower frequency band. The oscillators that may be used in the receiver, such as Rubidium clock and crystal oscillator, generally have the power-law noises with $\alpha = -2, -1, 0$ dominating during 1 s to 1 day (Allan 1987). So h_{-2}^{osc}, h_{-1}^{osc} and h_0^{osc} are the most important coefficients to describe the characteristics of the receiver's oscillator.

It is worth mentioned that the RT-PPP reference can be also seen as a virtual clock. The characteristics of the RT-PPP reference clock are combined from the satellite clocks, which are high-performance atomic clocks, including Hydrogen clocks, Cesium clocks, and Rubidium clocks. According to the evaluation of stability of the RT-PPP reference (Guo et al. 2022), these noises are focused on White Frequency Modulation (WFM) with $\alpha = 0$ power-law nosie during 1 s to 1 day. And the other noises can be ignored in the concerned time interval of Allan deviation. So h_0^{ref} is the most important coefficient to describe the characteristics of the RT-PPP reference clock. Thus, the system covariance matrix **Q** can be present as follows:

$$\mathbf{Q} = \begin{bmatrix} \frac{1}{2}(h_0^{\mathrm{osc}}+h_0^{\mathrm{ref}})\tau_0 + 2h_{-1}^{\mathrm{osc}}\tau_0^2 + \frac{2\pi^2}{3}h_{-2}^{\mathrm{osc}}\tau_0^3 & \pi^2 h_{-2}^{\mathrm{osc}}\tau_0^2 \\ \pi^2 h_{-2}^{\mathrm{osc}}\tau_0^2 & 2\pi^2 h_{-2}^{\mathrm{osc}}\tau_0 \end{bmatrix} \tag{14}$$

here, the system state covariance matrix **Q** is determined by the noise characteristics of the RT-PPP reference clock and the receiver oscillator.

The RT-PPP observation noise comes from the transmission and process of the GNSS signals, which can be seen as the white noise in phase. In this work, it is considered as the power-law noise with $\alpha = 2$, and can be expressed as follows:

$$R = h_2^{\mathrm{obs}} f_h/(2\pi)^2 \tag{15}$$

here, f_h is the measurement bandwidth. It is set to half of the sampling frequency in the RT-PPP observation. In practical applications, we can evaluate the noises through the time or frequency deviation sequences and fit these noise level figures with the ADEV.

Given the noise covariance of the state and observation equations, the bandwidth of the estimator is determined and proportional to Q/R. In the LQG system, the bandwidth of LQR is smaller than that of the estimator, and often decides the bandwidth of whole LQG. Thus, the actual state vector (Franklin et al. 2002) can be used to design the control law, which means that the RT-PPP observation noise is ignored, namely $R = 0$. Substituting the steady-state Kalman gain $\mathbf{K} = [\,1 \;\; 1/\tau_0\,]^T$ (Mishagin 2019) into (12), the transfer function (12) can be approximated as follows:

$$H(z) \approx \frac{z\left(g_1\tau_0+g_2\right)-g_2}{\left(z^2+\left(g_2+g_1\tau_0-2\right)z+1-g_2\right)} \tag{16}$$

Here, the control law gains g_1 and g_2 are the parameters of the transfer function.

Substituting $z = e^{s\tau_0}$ into the discrete-time transfer function, we can get the transfer function in the analog domain. When the bandwidth is small compared to the sampling rate $1/\tau_0$, the following first-order approximations are valid $z^{-1} \approx 1, 1 - z^{-1} \approx s\tau_0$ (Gardner 2005), the transfer function in the analog domain can be derived as follows:

$$H(s) \approx \frac{\frac{g_2}{\tau_0}s + \frac{g_1}{\tau_0}}{s^2 + \frac{g_2}{\tau_0}s + \frac{g_1}{\tau_0}} \tag{17}$$

Here, the system transfer function is a second-order low-pass filter, the damping ratio is $\xi = \frac{g_2}{2\sqrt{\tau_0 g_1}}$, and the undamped natural frequency is $\omega_n = \sqrt{\frac{g_1}{\tau_0}}$.

The amplitude response of the physical system does not cut off abruptly but has a transition band, resulting in multiple bandwidth definitions. In this article, we define the intersection of the system transfer function amplitude response and the system error transfer function amplitude response as bandwidth, namely $\left|H\left(j2\pi B_{\mathrm{L}}\right)\right| = \left|1 - H\left(j2\pi B_{\mathrm{L}}\right)\right|$. Using this definition, the bandwidth of the system can be obtained:

$$B_L = \frac{\sqrt{2} g_1}{2\pi \sqrt{\sqrt{4\tau_0^2 g_1^2 + g_2^4} - g_2^2}} \tag{18}$$

where the bandwidth B_L is a function of the control law gain g_1 and g_2, which are calculated from the cost matrices $\mathbf{W}_x$ and $\mathbf{W}_{\mathrm{u}}$ in (8) and (9). That means the bandwidth is decided by the cost parameters p, q, r.

Choosing a suitable steering interval τ_0 is important for a control system. According to the Nyquist sampling theorem, the system requires $B_{\mathrm{L}} = f_c$ to be smaller than $1/2\tau_0$Hz, namely $B_{\mathrm{L}} * \tau_0 < 0.5$. In addition, considering approximation from the analog domain to the digital domain, the product of B_L and τ_0 should be small enough, Satisfying $B_{\mathrm{L}} * \tau_0 < 0.033$ (Franklin et al. 1998). Considering the above, we propose to set B_L to the cross-point f_c and choose a τ_0 that makes $f_c * \tau_0$ a constant near 0.03. This is consistent with the reality that we understand. According to Fig. 3, f_c reduces when the oscillator gets more stable or the RT-PPP gets more unstable. In this case, increasing the steering interval is a good choice. In this article, we set the τ_0 to be an integral multiple of the RT-PPP observation period for simplicity.

As discussed above, in the cost matrices, r stands for control cost, p represents the cost of fractional frequency deviation, and q is the cost of time deviation. The three parameters are mutually influenced, and only two of them are independent variables. Multiply them by the same number, the control law does not change. Only the relative ratio between them is useful for the result of the control law. Thus, we can fix one of them as a constant to solve problem of system design. Since the phase cost has the dimension of τ_0^{-2}, and the frequency cost and control cost are dimensionless. We can set the phase cost as τ_0^{-2}, which makes the frequency cost and control cost the ratios of the phase cost. Thus, $p = \tau_0^{-2}$ is chosen in this work to eliminate the τ_0 effect in the formulations. In this situation, we still need some constraints to determine the parameters q, r, making the bandwidth to the expected value f_c.

From (18), it can be derived that the bandwidth B_{L} has the dimension of τ_0^{-1}. Thus, we can use $B_{\mathrm{L}}/\tau_0^{-1} = B_{\mathrm{L}} * \tau_0$ to describe the ratio of bandwidth to the sample frequency τ_0^{-1}, resulting in a unified description of systems with different sampling intervals. With regards to the parameter determination, it is difficult to formulate the relationship between the cost matrices and the bandwidth, however, contour map can visually describe this. Given $p = \tau_0^{-2}$, the contours of $B_L * \tau_0$ for different cost matrices parameters q and r are shown in Fig. 4. As shown in the figure, the value of $B_{\mathrm{L}} * \tau_0$ decreases as the control cost r increases. Its maximum value is $B_{\mathrm{L}} * \tau_0 \approx 0.2024$ when r and q reach their minimum values, $\log(r) = \log(q) = -10$, on the lower left corner. When control cost r is less than 1, i.e., $\log(r) < 0$, the value satisfies $0.15 < B_{\mathrm{L}} * \tau_0 < 0.2024$ for all the q in the range $-10 < \log(q) < 10$. As analyzed above, $B_L * \tau_0$ is supposed to be less than 0.033 in engineering applications. Hence, it is better to set r in the range $\log(r) > 0$, i.e., the ratio of control cost to phase cost is bigger than τ_0^2. When r is set in the range $\log(r) > 0$, the $B_{\mathrm{L}} * \tau_0$ is almost a constant if $\log(q) \leq 0$. That means system bandwidth is only influenced by the control cost r on the lower right plane. Moreover, the gradient of $B_{\mathrm{L}} * \tau_0$ to r is smaller than that on the upper right plane, which makes a high tolerance for the designing error and improve the robustness of the system. Thus, it is a good choice to choose control cost r on the lower right plane according to the desired bandwidth B_{L}.

The cost of the fractional frequency deviation q remains to be constrained. From Fig. 4, we can see that the bandwidth is not sensitive to it in the chosen area. However, the cost parameters q and r can directly influence the system damping ratio ξ, which is an important parameter paired with the bandwidth for second-order system. From the viewpoint of frequency domain, damping ratio determines

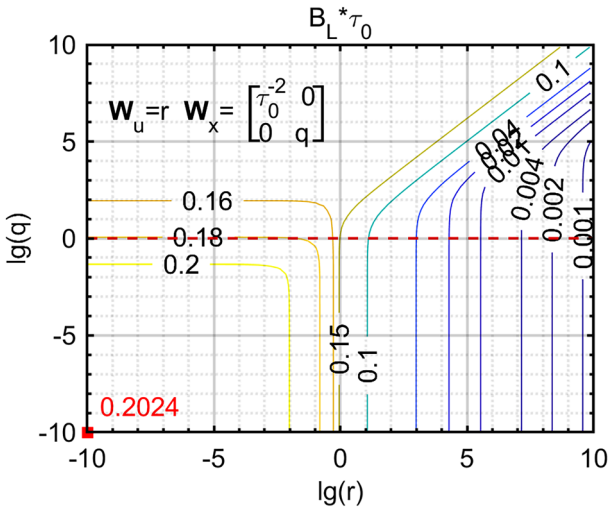

Fig. 4 Relationship between bandwidth and LQR cost parameters

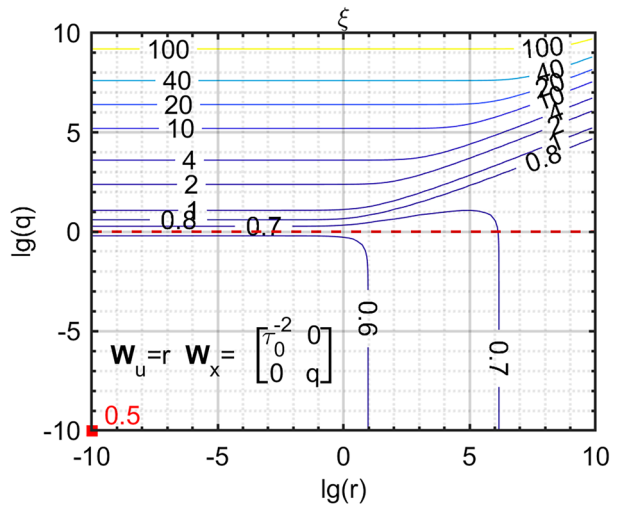

Fig. 5 Relationship between damping ratio and LQR cost parameters

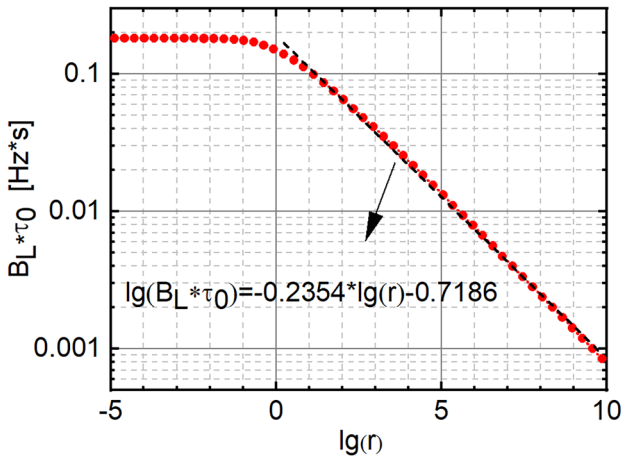

Fig. 6 Relationship between bandwidth and control cost

how an oscillation in a system damps after a disturbance. In the clock steering system, each adjustment to the clock frequency is a disturbance for the system. Given $p = \tau_0^{-2}$, the contours of damping ratio ξ for different cost parameters q and r is shown in Fig. 5. As shown in the figure, the damping ratio generally increases with the frequency cost q. For each fixed r, damping ratio ξ can traverse all the states, including underdamped, critically damped, and overdamped response. It can be seen clearly the fix value $q = 1$ makes damping ratio stay steadily at 0.6 to 0.8 as the control cost r increases. A damping ratio of 0.6 to 0.8 is usually reasonable for a second-order system. So $q = 1$ is chosen in this work.

Figure 6 shows the relationship between the bandwidth and the control cost r, which is the sectional view of the red dotted line ($q = 1$) in Fig. 4. As shown in the figure, $B_L * \tau_0$ remains steady when the control cost r is smaller than 1. While it decreases at a fixed slope for every 10 times increase in r. Then the relationship between the control cost r and $B_L * \tau_0$ when $r > 1$ can be fitted as follows,

$$\lg\left(B_L * \tau_0\right) \approx -0.2354 * \lg(r) - 0.7186 \tag{19}$$

Substituting $B_L = f_c$ into the formula above, we can get the value of r.

Results and discussions

To verify the clock steering performance and the parameter design method of LQG control, different noise level figures of various parts of the system are simulated. Meanwhile, the performances of RT-PPP timing with the designed clock steering method are evaluated and analyzed on a realized hardware platform.

Simulated experiments

Considering the behavior of different noise level figures of the oscillator, the GNSS satellite clock reference, and the GNSS observation in the clock steering system. Three different experiments presented in Table 1 is analyzed. The parameters of different experiments are designed using the proposed method. Meanwhile, the τ_0 is chosen according to the condition $f_c * \tau_0 < 0.033$ in all three experiments.

Figure 7 shows the PSD of the receiver oscillators and the GNSS references with observation noise adopted in the three experiments. It is worth mentioning that the noise of GNSS observation are considered together with that of the GNSS reference in the simulation to keep consistent with practice. It can be seen clearly from the figure that the cross section in Experiment 1 and Experiment 3 are almost the same, which means the control parameters are similar in the simulations. The simultaneous improvement of the GNSS reference and

Table 1 Simulated conditions with different noise level figures

Experiment	Receiver Oscillator	GNSS		Parameters	
	Osc $h_0^{osc}, h_{-1}^{osc}, h_{-2}^{osc}$	Ref h_0^{ref}	Obs R	B_L (Hz)	τ_0(s)
1(green)	1E − 24,2E − 24,1E − 26	3.631E − 21	1.252E − 20	0.0042	5
2(red)	1E − 24,2E − 24,1E − 26	3.631E − 23	1.252E − 22	0.031	1
3(blue)	1E − 26,2E − 26,1E − 28	3.631E − 23	1.252E − 22	0.0049	5

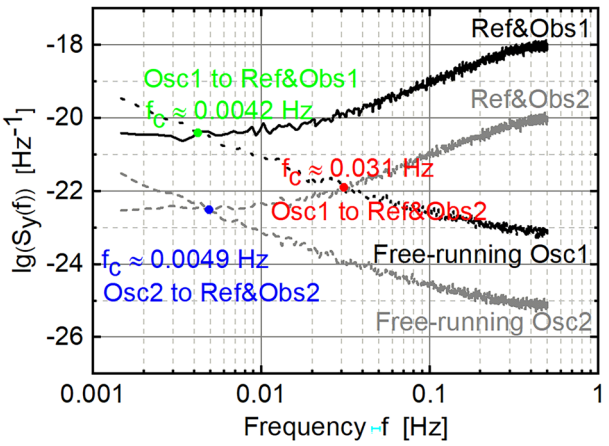

Fig. 7 Power spectral density of frequency fluctuation sources in clock steering system

the receiver oscillator in Experiment 3 relative to Experiment 1 results in similar control parameters. The quality relativity of the GNSS reference and the receiver oscillator determines the control parameters. And the bandwidth in Experiment 2 are almost 10 times bigger than that in the other two experiments, which means a faster correspondence in the clock steering.

Figure 8 shows the comparison of the steered oscillator phases compared to the reference phases in the three experiments. It can be seen that all the steered oscillator phases are consistent with their corresponding references. The standard deviations of the steered oscillator phases in the three experiments are 3.72 ns, 0.374 ns, 0.375 ns, respectively. The phase performances are improved if the noises of the references are reduced. Although the parameters in Experiment 1 are set to be similar to Experiment 3, the standard deviation with the better reference is smaller. That means the noises decide the output performance when the suitable parameters are designed. It also can be seen from the sub-figures that the phases in Experiment 1 and Experiment 3 are smoother than that of Experiment 2 due to the smaller bandwidth. The standard deviations of the differential phases of the steered oscillators and their corresponding references are 718 ps, 57 ps, and 64 ps. And the STD of differential phases in Experiment 2 is the smallest, for the bigger bandwidth makes it follow the reference clock closer and faster.

Figure 9 shows the overlapping Allan deviations of the GNSS references with observation noise, the free-running oscillators, and the steered oscillators under different conditions. As shown in the figure, all the steered oscillators combine the better short-term stability of the oscillator and the better long-term stability of the GNSS reference. Additionally, it is obvious that the steered oscillator in Experiment 2 has a better long-term stability than that in Experiment 1. This is because the noise level figures of the reference and observation in Experiment 2 are smaller than that in Experiment 1. The steered oscillator in Experiment 3 has a better short-term stability than that in Experiment 2 because of the smaller noise level figures of the oscillator. The proposed design method of the controller makes the frequency stabilities of the steered oscillators close to the limit at different noise level figures.

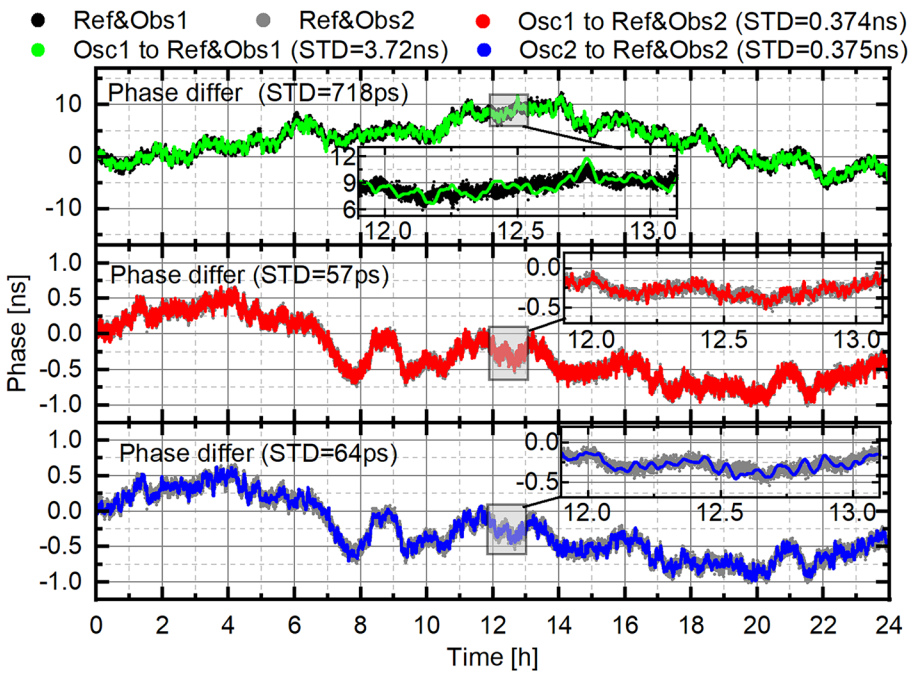

Fig. 8 Phases of steered oscillators with LQG controllers

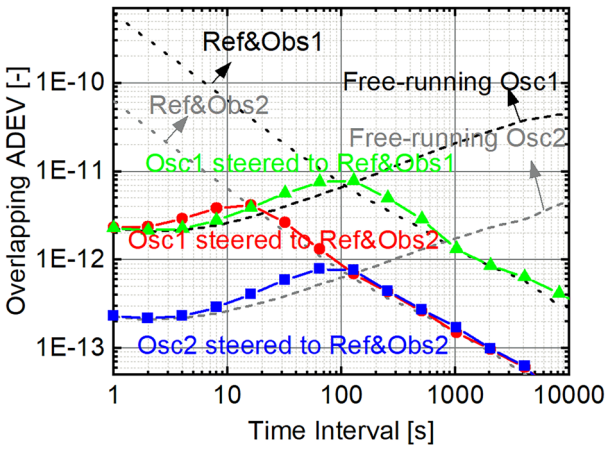

Fig. 9 Frequency stabilities of steered oscillators with LQG controllers

Real experiments

To evaluate the performances of the LQG controller and the RT-PPP timing, a RT-PPP timing receiver with a Rubidium clock is implemented using the proposed clock steering method. Figure 10 shows the setup for the real experiments. Phase noise test probe 3120A was used to measure the receiver's fluctuations. A high stable active Hydrogen maser (CH1-75A) was used as the measurement reference, whose stabilities described by Allan deviation are 2E-13@1 s and 7E-16@1 day, respectively. The RT-PPP ephemeris products from Wuhan University are adopted in the experiments. And the observations of the Global Positioning System (GPS) are employed.

A Rubidium clock, FE-5650A, is used as the oscillator of the timing receiver. The fluctuation sequence of the free-running Rubidium was measured using the phase noise test probe 3120A with the Hydrogen maser. To get the fluctuation sequence of the RT-PPP reference clock and observation, the Hydrogen maser was used as the clock of the timing receiver. Then the time deviation of the clock was estimated using RT-PPP. The Hydrogen maser is stable enough that the instability of time deviation sequence mainly comes from the RT-PPP reference and observation. Gaps and outliers

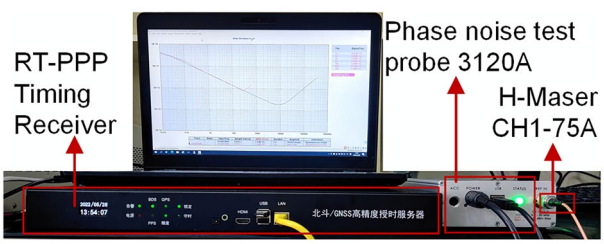

Fig. 10 Setup for real experiments

in the RT-PPP was handled before processing. The PSD of the fractional frequency fluctuations of the free running Rubidium and the RT-PPP reference with observation are shown in Fig. 11. It can be seen that the point of intersection frequency f_c is about 0.0045Hz. Setting the steering interval $\tau_0 = 5$s, the control cost can be calculated $r = 8859$ according to (19), which corresponds to the control law $\mathbf{G} = \begin{bmatrix} 0.0020 & 0.1360 \end{bmatrix}$.

Using the fluctuation sequences, the Allan deviation of the free-running Rubidium clock and RT-PPP could be evaluated. The linear frequency drift of the Rubidium clock is removed. And the noise level figures can be estimated (Riley and Howe 2008): $h_0^{\text{osc}} \approx 3.74 * 10^{-23}$, $h_{-1}^{\text{osc}} \approx 1.30 * 10^{-26}$, $h_{-2}^{\text{osc}} \approx 2.07 * 10^{-30}$. The noise level figures of RT-PPP reference and observation can be fitted using the combined fluctuation sequence:$h_0^{\text{ref}} \approx 1.47 * 10^{-23}$, $R = 3.21 * 10^{-22}$. With these parameters, a complete LQG controller is realized, and the performance of the steered clock is evaluated.

Figure 12 shows the time precision and frequency accuracy of the steered RT-PPP receiver. As described above, Hydrogen maser is used as the external reference in the evaluation. The internal time deviation reflects the deviation and jitter of the receiver clock relative to the RT-PPP reference clock. Results show that the internal time deviation estimated by RT-PPP fluctuates between -0.2 and 0.2 ns, whose standard deviation is 0.05 ns. The external time deviation compared to the Hydrogen maser is between -0.6 and 0.5 ns with standard deviation 0.21 ns. It is the timing precision of the receiver providing to the user, including the errors coming from the hardware of timing receiver and the Hydrogen maser. The output frequency deviations of the timing receiver are measured for each second. It is within $\pm 2 * 10^{-11}$. The frequency accuracy could be estimated using its mean, which is about $8.92 * 10^{-15}$.

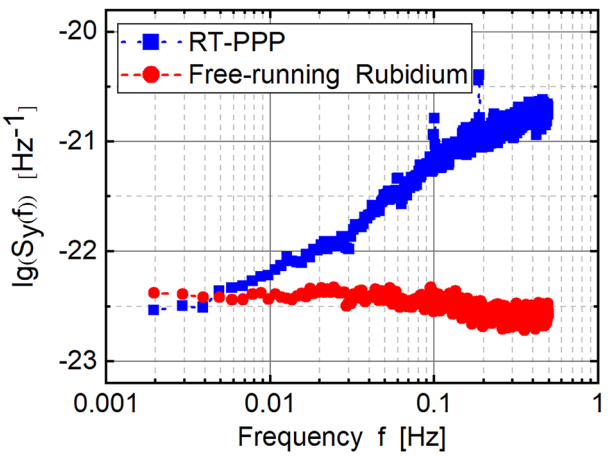

Fig. 11 Power spectral density of frequency fluctuations of free-running Rubidium clock and RT-PPP

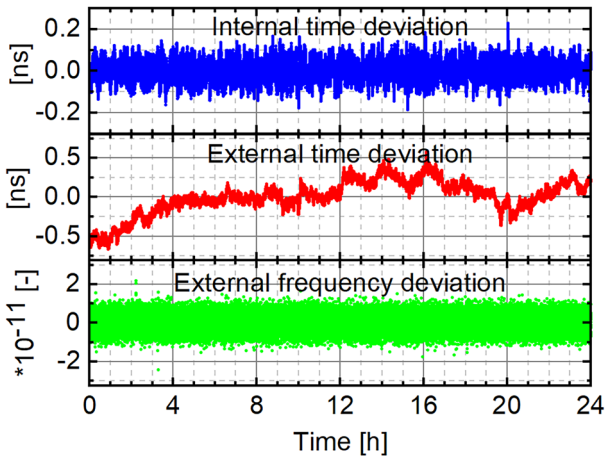

Fig. 12 Time and frequency precision of the steered RT-PPP receiver

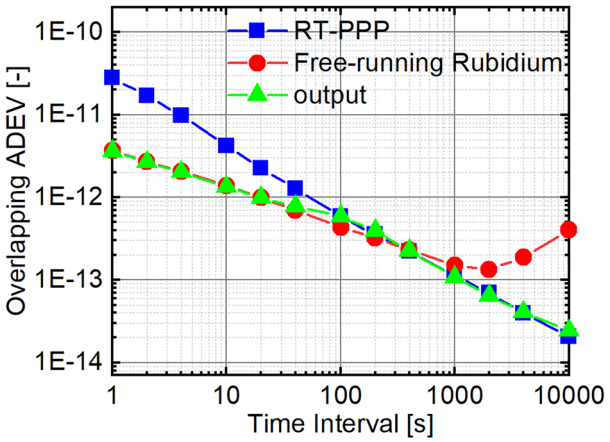

Fig. 13 Frequency stability of the steered RT-PPP timing receiver

To evaluate the frequency stability of the steered clock, the overlapping Allan deviation of the receiver output frequency is shown in Fig. 13. As shown in Fig. 13, the free-running Rubidium clock has a better short-term stability than RT-PPP reference. However, it deteriorates when the measured interval is more than 1000 s. In contrast, the RT-PPP reference has a worse short-term stability but a better long-term stability. It can be seen clearly that the OADEV curve of the output almost coincidences that of the free-running Rubidium clock in the short-term stability and that of the RT-PPP reference in the long-term stability. Thus, the steered RT-PPP timing receiver has the optimal frequency stability as expected. The stabilities at 1 s and 10,000 s are 3.59E-12@1 s and 2.43E-14@10000s, which is more stable than a high-quality Cesium clock (5071A).

Conclusions

This article focuses on the LQG clock steering parametric design for the RT-PPP timing receiver to output high-precision time and stable frequency. The goal of clock steering parametric design is to bring the performance close to the limits of the precision of the free-running oscillator, the GNSS RT satellite clock reference and the GNSS observation. We analyze the structure and theoretically derive the transfer function of the clock steering system. Then, the design method of the clock steering parameters is proposed using the separation principle of the control theory. The bandwidth and damping ratio in the frequency domain are used as constraints to the design control parameters. Simulated results show that the parametric design method is feasible for different noise conditions. Experimental results with a Rubidium clock RT-PPP timing receiver show that the proposed clock steering method optimally combines the short-term stability of the Rubidium clock and the long-term stability of the RT-PPP expectedly. The precision of output 1PPS is 0.21 ns over 24 h. And the frequency stabilities can reach 3.59E-12@1 s and 2.43E-14@10000 s, which is more stable than a high-quality Cesium clock.

Considering details in each part of the system, the control parameter design is always complex. Thus, it is more common to present parametric design results rather than parametric design procedures. And it is difficult to apply a proposed controller to another case. We presented a relatively complete and detailed control parameter design process for the GNSS timing receiver. Although the results of parameter design may not be directly applied to various receivers, the idea of parameter design can be used in different situations.

Acknowledgements This work was supported by the National Key Research and Development Program of China under Grant 2021YFB3900703 and the National Natural Science Foundation of China under Grant 42227802, 41974038, 42174029, and 41931075.

Author contributions Author WG and SG designed the research; WG, MZ, HZ, and SG performed the research; WG, MZ, and SG analyzed the result; WG, MZ, and SG drafted the paper. All authors discussed, commented on, and reviewed the manuscript.

Funding This work was supported by the National Key Research and Development Program of China under Grant 2021YFB3900703 and the National Natural Science Foundation of China under Grant 42227802, 41974038, 42174029, and 41931075.

Data availability The datasets generated during and/or analyzed during the current study are available from the corresponding author on reasonable request.

Declarations

Conflict of interest The authors have no competing interests to declare that are relevant to the content of this article.

Consent for publication The work described has not been published before; that it is not under consideration for publication anywhere else; that its publication has been approved by all co-authors, if any, as well as by the responsible authorities—tacitly or explicitly—at the institute where the work has been carried out.

References

Allan DW (1987) Time and frequency (time-domain) characterization, estimation, and prediction of precision clocks and oscillators. IEEE Trans Ultrason Ferroelectr Freq Control 34(6):647–654. https://doi.org/10.1109/t-uffc.1987.26997

Franklin GF, Powell JD, Emami-Naeini A, Powell JD (2002) Feedback control of dynamic systems, vol 4. Prentice hall, Upper Saddle River

Franklin GF, Powell JD, Workman ML (1998) Digital control of dynamic systems, vol 3. Addison-Wesley, Reading

Gardner FM (2005) Phaselock techniques. Wiley, Sons

Guo W, Zuo H, Mao F, Chen J, Gong X, Gu S, Liu J (2022) On the satellite clock datum stability of RT-PPP product and its application in one-way timing and time synchronization. J Geodesy 96(8):52. https://doi.org/10.1007/s00190-022-01638-5

Guo W, Song W, Niu X, Lou Y, Gu S, Zhang S, Shi C (2019) Foundation and performance evaluation of real-time GNSS high-precision one-way timing system. GPS Solut 23:1–11. https://doi.org/10.1007/s10291-018-0811-1

Hajimiri A (2001) Noise in phase-locked loops. In: 2001 Southwest Symposium on Mixed-Signal Design (Cat. No. 01EX475) (pp. 1–6). IEEE. https://doi.org/10.1109/SSMSD.2001.914927

Koppang P, Leland R (1999) Linear quadratic stochastic control of atomic hydrogen masers. IEEE Trans Ultrason Ferroelectr Freq Control 46(3):517–522. https://doi.org/10.1109/58.764838

Koppang, P., Johns, D., Skinner, J. (2003). Application of Control Theory in the Formation of a Timescale. Proceedings of ION PTTI 2003, Institute of Navigation, San Diego, California, USA, December 2–4, (pp. 319–326)

Kroupa V (1982) Noise properties of PLL systems. IEEE Trans Commun 30(10):2244–2252. https://doi.org/10.1109/TCOM.1982.1095404

Kusters JA (1996) The global positioning system and HP smartclock. Hewlett Packard Journal 47(6):60–67

Matsakis D (2019) The effects of proportional steering strategies on the behavior of controlled clocks. Metrologia 56(2):025007. https://doi.org/10.1088/1681-7575/ab0614

Mishagin KG, Lysenko VA, Medvedev SYE (2019) A practical approach to optimal control problem for atomic clocks. IEEE Trans Ultrason Ferroelectr Freq Control 67(5):1080–1087. https://doi.org/10.1109/TUFFC.2019.2957650

Ramachandran D, Din AHM, Ibrahim SA, Omar AH (2019) Real-time precise point positioning (RT-PPP) for positioning and mapping. In: GCEC 2017: Proceedings of the 1st Global Civil Engineering Conference 1 (pp. 891–913). Springer Singapore. https://doi.org/10.1007/978-981-10-8016-6_64

Riley WJ, Howe DA (2008) Handbook of frequency stability analysis. NIST Sp

Rønningen OP, Danielson M (2019) A novel PPP disciplined oscillator. In: 2019 Joint Conference of the IEEE International Frequency Control Symposium and European Frequency and Time Forum (EFTF/IFC) (pp. 1–4). IEEE. https://doi.org/10.1109/FCS.2019.8856034

Wu Y, Gong H, Zhu X, Ou G (2016) A DPLL method applied to clock steering. IEEE Trans Instrum Meas 65(6):1331–1342. https://doi.org/10.1109/TIM.2016.2526699

Publisher's Note Springer Nature remains neutral with regard to jurisdictional claims in published maps and institutional affiliations.

Springer Nature or its licensor (e.g. a society or other partner) holds exclusive rights to this article under a publishing agreement with the author(s) or other rightsholder(s); author self-archiving of the accepted manuscript version of this article is solely governed by the terms of such publishing agreement and applicable law.

Wenfei Guo received his B.E. degree in communication and information system from Wuhan University of Technology, Wuhan, China in 2004, and his PhD degree in communication and information system from Wuhan University, Wuhan, China, in 2011. From 2012 to 2015, he was a Postdoctoral Researcher with the GNSS Research Center, Wuhan University (WHU). He worked as a Visiting Fellow with the Australian Centre for Space Engineering Research (ACSER), University of New South Wales (UNSW), from 2017 to 2018. Since 2022, he has been a Professor with the GNSS Research Center, Wuhan University (WHU). His research interests include GNSS receivers and related signal processing technologies, including high-precision timing receivers, anti-jamming receivers, GNSS-R technologies, etc.

Mengmeng Zhu received her B.Sc. degree from Wuhan University in 2020 and is currently a student at GNSS Research Center, Wuhan University, where she is pursuing the master's degree. Her current research interest includes high precise timing receivers.

Shengfeng Gu received his Ph.D. degree from the GNSS Research Center of Wuhan University in 2013 and is currently a Professor at GNSS Research Center, Wuhan University. His current research mainly focuses on multi-GNSS data processing, multi-sensor navigation and real-time ionospheric modeling.

Hongming Zuo received his B.Sc. degree from Chongqing University in 2020 and is currently a student at GNSS Research Center, Wuhan University, where he is pursuing the master's degree. His current research interest includes high precise timing receivers.

Jingnan Liu is member of Chinese Academy of Engineering, professor at Wuhan University and expert in geodesy and surveying engineering with the specialty of GNSS technology and applications. He has been the head of the National Engineering Research Center for Satellite Positioning System since 1998. He is currently an executive member of the council, Chinese Society for Geodesy Photogrammetry and Cartography, the editorial board member of GPS World and the coordinator of the International GPS Geodynamics Services. He has published more than 150 academic papers and supervised more than 100 postgraduates.